Teleoperation system with 6-DoF haptic feedback for aerial manipulation

Kotaro Kaneko[1,2] , Junichiro Sugihara[1], Jinjie Li[1], and Moju Zhao[1]

***Abstract*— Aerial manipulations using aerial robots are gaining attention for their work in high places and hazardous locations. While autonomous control of robots has advanced, teleoperation by human operators is still necessary for tasks in complex and unknown environments. In such teleoperation, haptic feedback that allows the operator to perceive the forces exerted on the robot is important. In many cases, underactuated multirotors are used for teleoperation, but the use of fully actuated multirotors is advancing for more complex tasks. Conventional teleoperation methods cannot achieve both intuitive control corresponding to the increased degrees of freedom and feedback of all 6-dimensional force and torque. Therefore, in this study, we propose an operating device capable of expressing 6-dimensional force and torque, and a teleoperation system that makes it easy to perform work remotely using a fully actuated multi-rotor. The operating device has a floating base with a thrust and vectoring mechanism, enabling independent control of position and attitude and independent presentation of forces and torques. The teleoperation system has *Position Mapping Mode* and *Velocity Mapping Mode* settings, enabling both rapid movement in a wide area and precise movement for work. We verified the effectiveness of the proposed method for aerial telemanipulations through experiments cleaning tilted walls. Our new framework contributes to the realization of more complex aerial tasks using aerial robots.**

Fig. 1. Using a novel device that provides haptic feedback of 6-dimensional force and torque, human operator is teleoperating a fully actuated aerial robot to clean tilted wall by using the device

I. INTRODUCTION

Recently, aerial manipulation has been attracting increasing attention. The high maneuverability and broad working space of aerial robots enable work in remote areas and in locations that are difficult for humans to access. They also enable contact work in locations that are dangerous for human operators, such as high altitudes and locations where harmful substances are suspended in the air. The ideal scenario is for robots to operate completely autonomously, and research on autonomous control has made remarkable progress [1]. However, due to the complexity and numerous disturbances in aerial work environments, it is necessary to include human operators in the loop [2]. By utilizing human's ability to make appropriate judgments, it becomes possible to perform optimally in real time, even in unknown environments or with unknown work objects. For this reason, research on the teleoperation of aerial robots has been advanced. Most of these research focus on conventional underactuated multi-rotors [3]–[6]. Underactuated multi-rotors have 4 degrees of freedom (DoF), consisting of 3 degrees of translational motion and 1 degree of rotational motion, and can be controlled using conventional joystick-like devices. On the other hand, research on fully actuated multi-rotors is also being advanced to improve the DoF in aerial operations [7]–[9]. These robots have 6-DoF for control, including 3-dimensional translation and 3-dimensional rotation, so new types of devices are required to operate them. In [10], the operator uses a robot arm fixed to the ground as a operating device. While this proposed device allows for 6-dimensional independent input, it has the drawback of being difficult to move because its base is fixed. On the other hand, a floating operating device that senses the position and posture of the human hand to obtain operating input is proposed in [11]. With this method, there is no need to fix part of the operating device, so it does not interfere with the operator's hand movements. For this reason, floating devices are suitable for teleoperation of fully actuated aerial robots.

In teleoperation, feedback of information from the robot to the operator is essential. Especially in manipulations involving contact with the external environment, haptic feedback is important for smooth operation. Haptic feedback used in many studies is simple, such as vibration. However, in order to perform work smoothly, it is desirable to express the force applied to the tool as force. For example, a device that can apply 3-dimensional force to the handle by using 6 propellers is proposed in [12]. In addition, a

[1]DRAGON Lab, Department of Mechanical Engineering, The University of Tokyo, Tokyo 113-8654, Japan {sugihara, jinjie-li, chou}@dragon.t.u-tokyo.ac.jp

[2]HNL Lab, Department of Mechanical Engineering, The University of Tokyo, Tokyo 113-8654, Japan kaneko@hnl.t.u-tokyo.ac.jp

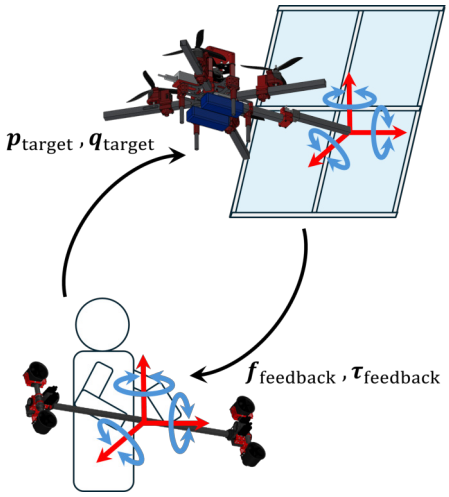

Fig. 2. Diagram of our proposed teleoperation system. p_{target} and q_{target} are target position and quaternion of the aerial robot, f_{feedback} and τ_{feedback} are feedback forces and torques.

device that provides 1-direction force and 2-direction torque by attaching two quadrotors to both ends of a long rod is proposed in [13]. These studies have succeeded in presenting forces and torques to the operator without fixing the base, but they are unable to present all 6-dimensions forces and torques independently. Therefore, this study proposes a floating device that can present all wrenches, 6-dimensional vectors arranged vertically with 3-dimensional force and 3-dimensional torque, independently.

The overall diagram of the proposed teleoperation system is shown in Fig.2. The contributions of this study are as follows.

- We propose a floating teleoperating device that can independently present all 6-dimensional wrenches to the operator.
- We propose a teleoperation system equipped with 6-dimensional wrench feedback that can simultaneously control all DoF of a fully driven aerial robot, enabling both precise and long-distance operations.
- We verified the effectiveness of the proposed system through experiments including obstacle avoidance and cleaning tilted walls.

II. TELEOPERATION DEVICE

A. Design of Device

The teleoperation device proposed in this research enables operators to perform tasks through remote aerial robots easily. Most tasks performed by humans require the use of some kind of tool. Humans interact with the external environment through the handles of these tools and obtain information about the reaction forces. Therefore, when performing tasks remotely, it is most intuitive to grip and operate the device as if the robot's tools were physically present in the operator's hands.

As mentioned in Sec. I, in teleoperation using aerial robots, the device must be capable of floating and independently providing 6-dimensional wrench. To achieve these

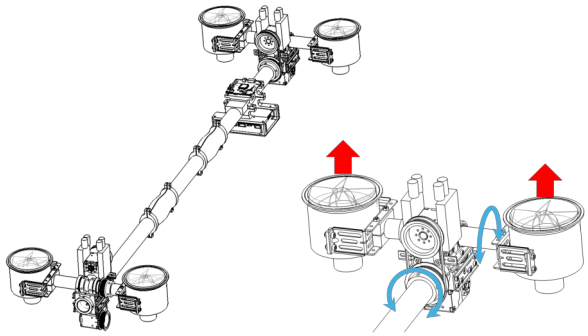

Fig. 3. Hardware design of proposed teleoperation device. Left:Whole view. Right:Thrust vectoring mechanism. The red arrows mean the thrust, and blue arrows is the rotational direction.

functions, we use thrust and a thrust vectoring mechanism. The thrust vectoring mechanism is a modified version of the one proposed by Zhao et al [14]. As shown in the right of Fig. 3, this thrust vectoring mechanism can rotate in 2 directions. By attaching 2 rotors that generate thrust at both ends, it has a total of 4-DoF. By attaching this module to both ends of a long rod modeled like a tool, the device as a whole can obtain 8-DoF for control input. Since this is larger than the dimension 6 of the wrench we want to present, it allows us to present all wrenches with redundancy.

B. Control of Device

All of the following is considered in a coordinate system fixed to the device. The DoF of control of this device are as shown on the top side of Fig. 4, but consider a virtual thrust as shown on the bottom side of Fig. 4. The allocation matrix from virtual thrust to desired wrench can be expressed as

$$Q_1 = \begin{pmatrix} I_3 & I_3 \\ skew(\boldsymbol{p}_{f_{\text{v1}}}) & skew(\boldsymbol{p}_{f_{\text{v2}}}) \end{pmatrix}, \tag{1}$$

where $I_3 \in R^{3\times3}$ is identity matrix, $\boldsymbol{p}_{f_{\text{v}i}}$ is position vector of the virtual thrust $f_{\text{v}i}$ point in the coordinate system of the handle, and $skew(\boldsymbol{p})$ is skew-symmetric matrix of $\boldsymbol{p}$. The virtual thrust $\boldsymbol{f}_{\text{v}} = [\boldsymbol{f}_{\text{v1}}, \boldsymbol{f}_{\text{v2}}]^T$ is calculated from the desired wrench after removing torque around x-axis $\boldsymbol{W}_{\text{des}} = [F_{\text{des}x}, F_{\text{des}y}, F_{\text{des}z}, T_{\text{des}y}, T_{\text{des}z}]^T$ as follows.

$$\boldsymbol{f}_{\text{v}} = Q_1^{\#}(\boldsymbol{W}_{\text{des}} + \boldsymbol{g}), \tag{2}$$

where $\boldsymbol{g} = [0, 0, Mg, 0, 0, 0]^T$ is the gravity term, which is the product of the mass of the device M and the gravitational acceleration. And $Q_1^{\#} \in R^{6\times5}$ is the pseudo-inverse of Q_1 with excluding the 4th row corresponding to torque around the x-axis. The vectoring angles is calculated as follows:

$$\theta_i = \arctan\left(-\frac{f_{\text{v}iy}}{f_{\text{v}iz}}\right), \tag{3}$$

$$\phi_i = \arctan\left(\frac{f_{\text{v}ix}}{-f_{\text{v}iy}\cdot\sin(\theta_i) + f_{\text{v}iz}\cdot\cos(\theta_i)}\right). \tag{4}$$

When moving the vectoring mechanism, the following counter torque occurs around the x-axis.

$$\tau_{\text{counter}} = \sum I_i\ddot{\theta}_i, \tag{5}$$

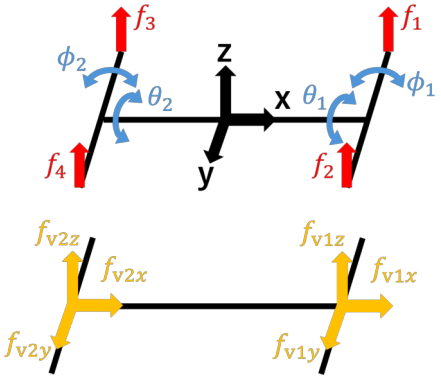

Fig. 4. Top:Control DoF of the proposed device. The black allows shows the hadle coordinate system fixed on the device. Bottom:Virtual thrust considered on a control model.

where I_i is the ineria of the vectoring module around x-axis.

The allocation matrix from virtual thrust and torque around x-axis to the actual thrust can be expressed as

$$Q_2 = \begin{pmatrix} 1 & 0 & 1 & 0 \\ 0 & 1 & 0 & 1 \\ d_1 \cos\psi_1 & d_2 \cos\psi_2 & -d_3 \cos\psi_1 & -d_4 \cos\psi_2 \end{pmatrix}, \tag{6}$$

where d_1, d_2, d_3, d_4 is the distance from each rotor to the longitudinal axis of the device. Then, the actual thrust $\boldsymbol{f} = [f_1, f_2, f_3, f_4]^T$ is calculated as follows:

$$\boldsymbol{f} = Q_2^{\#} \begin{bmatrix} |\boldsymbol{f}_{\mathrm{v1}}| \\ |\boldsymbol{f}_{\mathrm{v2}}| \\ T_{\mathrm{des}x} + \tau_{\mathrm{counter}} \end{bmatrix}, \tag{7}$$

where $Q_2^{\#} \in R^{4\times3}$ is the pseuso-inverse of Q_2. Since the range of force that can be exerted by the rotor is limited, the solution obtained here is not always feasible. If the solution is outside the feasible range, substitute the closest feasible value and recalculate the solution.

III. TELEOPERATION SYSTEM

This chapter describes a teleoperation system for performing tasks using a fully actuated aerial robot. The system consists of generating position commands from the operator to the robot and generating force feedback from the robot to the operator.

A. Position Operating Command

Two main functions are required to control the position of an aerial robot. One is long-distance movement, which is the function of quickly moving within the almost infinite movement space available to the aerial robot. The other is precise movement, which is a function for performing detailed tasks accurately. To achieve both of these functions, we developed two operating modes: *Position mapping mode* and *Velocity mapping mode*.

1) Position Mappng Mode: We propose *Position Mapping Mode* for precise tasks. In this mode, the target position $\boldsymbol{p}_{\mathrm{target}}$ and quaternion $\boldsymbol{q}_{\mathrm{target}}$ is generated as follows:

$$\boldsymbol{p}_{\mathrm{target}} = \boldsymbol{p}_{\mathrm{robot}}(t_0) + \boldsymbol{k}_1 \odot (\boldsymbol{p}_{\mathrm{device}}(t) - \boldsymbol{p}_{\mathrm{device}}(t_0)), \tag{8}$$

$$\boldsymbol{q}_{\mathrm{target}} = \boldsymbol{q}_{\mathrm{device}}(t), \tag{9}$$

where t_0 refers to the moment of entering this mode, and $\odot$ is the Hadamard product, which is the product of each element of the vector. And $\boldsymbol{k}_1$ is a scaling parameter that can be adjusted as appropriate depending on the task type.

2) Velocity Mappng Mode: On the other hand, we propose *Velocity Mapping Mode* for long-distance movement. In this mode, the target position $\boldsymbol{p}_{\mathrm{tar}}$ and quaternion $\boldsymbol{q}_{\mathrm{tar}}$ is generated as follows:

$$\boldsymbol{p}_{\mathrm{target}} = \boldsymbol{p}_{\mathrm{robot}}(t) + \boldsymbol{k}_2 \odot (\boldsymbol{p}_{\mathrm{device}}(t) - \boldsymbol{p}_{\mathrm{device}}(t_0)), \tag{10}$$

$$\boldsymbol{q}_{\mathrm{target}} = \boldsymbol{q}_{\mathrm{robot}}(t) + \boldsymbol{k}_3 \odot (\boldsymbol{q}_{\mathrm{device}}(t) - \boldsymbol{q}_{\mathrm{device}}(t_0)), \tag{11}$$

where $\boldsymbol{k}_2$ and $\boldsymbol{k}_3$ are scaling parameters. Adding the amount of change in the device to the robot's position and quaternion at each time point is equivalent to controlling the robot's velocity.

In this mode, it is important for the operator to recognize the initial origin of the device, as well as when operating with a joystick. The device proposed in this study enables the operator to recognize the origin by providing a reaction force corresponding to the amount of movement from the origin of the device. If the magnitude of the feedback force is made proportional to the amount of device movement, as with commands and control, the force near the origin becomes small, making it easy to lose sight of the origin. Therefore, logarithmic conversion is used as follows:

$$\boldsymbol{f}_{\mathrm{feedback}} = \log(\boldsymbol{k}_4 \odot (\boldsymbol{p}_{\mathrm{device}}(t) - \boldsymbol{p}_{\mathrm{device}}(t_0))), \tag{12}$$

$$\boldsymbol{\tau}_{\mathrm{feedback}} = \log(\boldsymbol{k}_5 \odot (\boldsymbol{q}_{\mathrm{device}}(t) - \boldsymbol{q}_{\mathrm{device}}(t_0))), \tag{13}$$

where $\boldsymbol{k}_4$ and $\boldsymbol{k}_5$ are scaling parameters. This conversion increases the feedback force near the origin, making it easier to recognize the origin. In addition, in order to reduce the difficulty of operation, *Stop Zone* where no commands are sent to the robot is set near the origin.

By using these two modes appropriately, it is possible to perform tasks quickly and precisely in a large workspace.

B. Feedback of Force and Torque

The working end effector of an aerial robot is subject to 6 degrees of force and torque. In order to perform tasks smoothly, the operator must correctly recognize these 6 dimensional forces and torques. Research by Stevens et al. [15] has shown that there is a relationship between the magnitude of change in human perception and the magnitude of actual physical stimulation, as shown below:

$$\Phi(I) = kS^{\alpha}, \tag{14}$$

where I is the intensity of strength of the physical stimulus, $\Phi(I)$ is the magnitude of the sensation evoked by the stimulus, and k is proportionality constant. And it has been

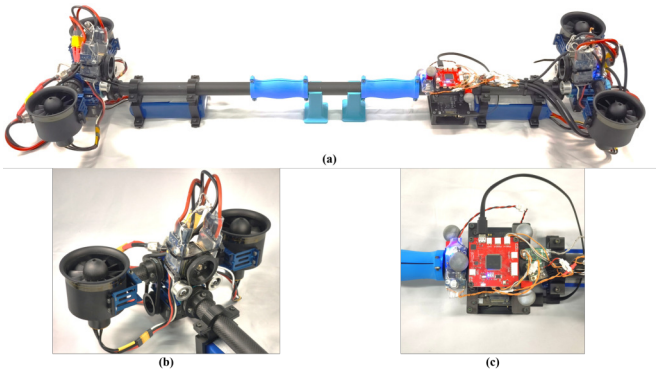

Fig. 5. Snapshot of self-designed teleoperation device. (a) is the whole view. (b) is the 2-Dof thrust vectoring mechanism. (c) is the reflective markers for Motion Capture system.

Fig. 6. Snapshot of fully actuated aerial robot. This is modefied version of the *BEATLE* proposed in [16].

reported that α depending on the type of stimulation, and it is 1.45 when recognizing gravity with the entire arm. The device proposed in this study provides force feedback to the operator's entire arm, so the physical stimulus is considered to be the same.

To enable the operator to correctly recognize changes in wrench, it is important to cancel this exponential relationship and make the perception linear. Thus, the wrench presented to the operator is generated from the wrench applied to the robot's manipulator as follows.

$$\boldsymbol{w}_{\text{feedback}} = \log_{\alpha}(\boldsymbol{k}_7 \odot \boldsymbol{w}_{\text{measured}}), \tag{15}$$

where $\boldsymbol{w}_{\text{feedback}}$ is a wrench that feedback to the operator, and $\boldsymbol{w}_{\text{measured}}$ is a wrench that is measured at the end effector of the robot, and $\boldsymbol{k}_7$ is a parameter that adjusts the magnitude.

IV. EXPERIMENTS

A. Setup

As shown in Fig. 5, we built the teleoperation device described in Sec. II. The device weighs $3.075\,\mathrm{kg}$, and with the battery installed, it weighs $3.969\,\mathrm{kg}$. Its dimensions are $1.033\,\mathrm{m}$ in length, $0.296\,\mathrm{m}$ in width, and $0.215\,\mathrm{m}$ in height. Dynamixel XH430-W350 is used as the actuator to rotate the thrust vectoring mechanism. The robot to be operated is a modified version of the fully actuated aerial robot proposed in [16], as shown in Fig. 6. Compared to the original robot *BEATLE Module* in [16], the *Docking Mechanism* and *Housing* have been removed, and the end effector for cleaning and Leptorino CFS018CA201U force sensor have been installed. Since the core of this experiment is to verify a teleoperation system using 6-dimensional wrench feedback, we use the Optitrack Motion Capture system to obtain the position and posture of the device and robot in order to simplify the experiment.

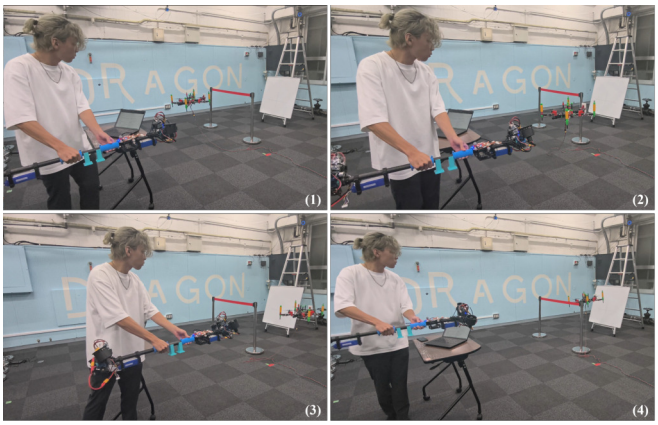

Fig. 7. Continuas snapshot of the obstacle avoidance with *Velocity Mapping Mode*.

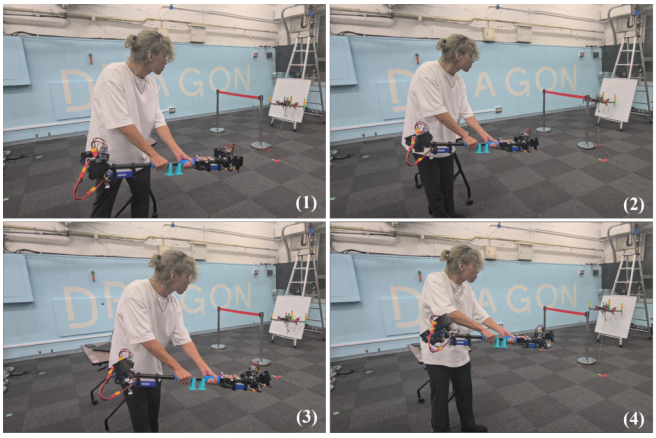

Fig. 8. Continuas snapshot of the wall cleaning with *Position Mapping Mode*.

B. Procedure

In order to verify the effectiveness of our proposed teleoperation system, we designed an experiment that simulates cleaning the walls of a tall building. In this experiment, as shown in Fig. 7 and Fig. 8 the operator uses *Velocity Mapping Mode* to avoid obstacle and move long distances to the work area, and then uses *Position Mapping Mode* to wipe ink on a whiteboard that simulates dirt on the wall. The wall surface to be cleaned is tilted from the vertical, which is a difficult task for a conventional under-actuated aerial robot. In this experiment, the wall surface is tilted approximately $15.6°$ from the vertical. The experiment was conducted in a space measuring $7\,\mathrm{m}$ in length, $6\,\mathrm{m}$ in width, and $2\,\mathrm{m}$ height. Due to the insufficient height of the experimental space, *Velocity*

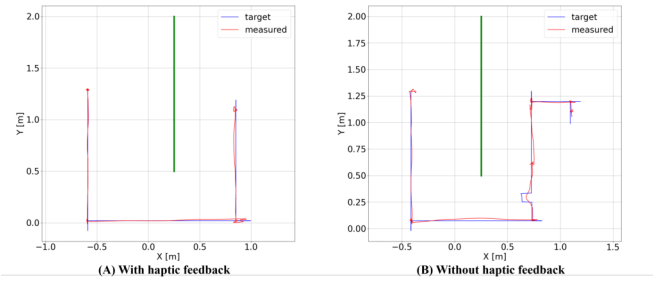

Fig. 9. Robot trajectory for the obstacle avoidance with *Velocity Mapping Mode*. The green line means obstacle. The horizontal tracking RMSE are (A):X:0.062 m and Y:0.065 m, and (B):X:0.047 m and Y:0.060 m.

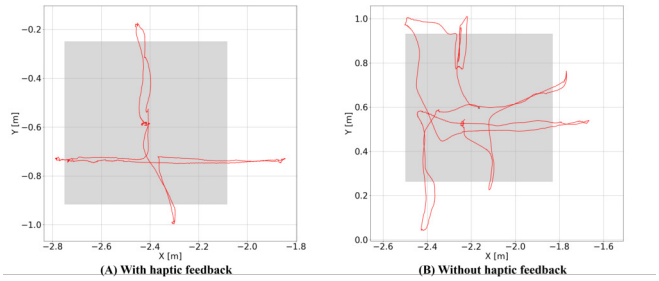

Fig. 10. Device trajectory for the obstacle avoidance with *Velocity Mapping Mode*. The gray area has a radius of 0.33 m and is *Stop Zone* where no commands are sent to the robot.

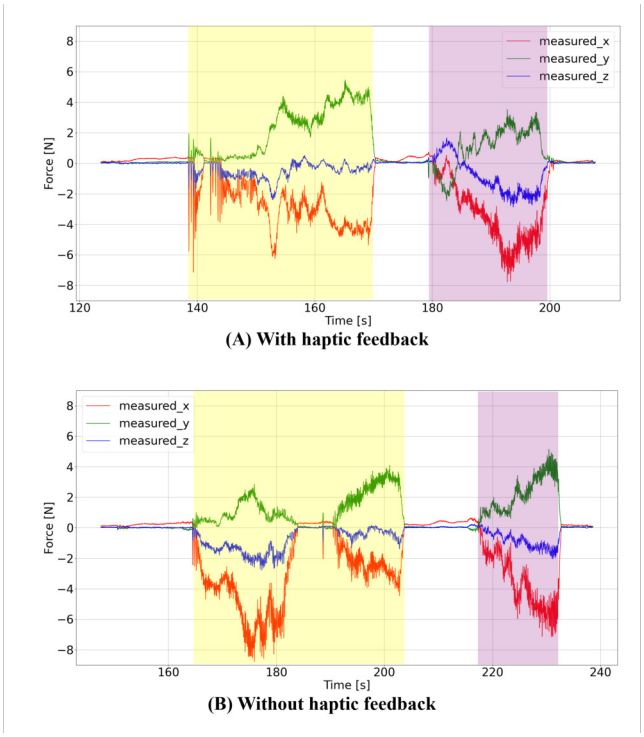

Fig. 11. Force values measured by force sensor attached to the end effector. The yellow highlighted area shows the process in which the robot moved horizontally, and the purple highlighted area shows the process in which the robot moved vertically.

Mapping Mode was not used for the vertical operation of the aerial robot. This experiment was conducted in two ways: (A) using haptic feedback from the device and (B) without using haptic feedback.

C. Result and Discussion

In the experiment, the operator used *velocity mapping mode* to avoid obstacles as shown in Fig. 7 and *position mapping mode* to clean the tilted wall as shown in Fig. 8. In each case, we compared (A) with haptic feedback and (B) without haptic feedback.

1) Obstacle Avoidance: Fig. 9 shows the trajectory of the robot, and Fig. 10 shows the trajectory of the device during operation. The RMSE of the robot's trajectory is slightly smaller in (B) than in (A), but both are small enough not to give the operator an unintuitive impression. As shown in Fig. 9, a change in the direction of movement occurs near (x,y) = (0.75 m, 0.25 m) in (B). This is thought to be because the operator could not correctly recognize the origin of the *Stop Zone* and unintentionally operated it in the -x direction, and then tried to correct it. In addition, in both cases (A) and (B), it was difficult for the operator to recognize the distance between the obstacle and the robot. This was because the operator, robot, and obstacle were aligned in a straight line, suggesting the need for a function that allows the operator to freely move the viewpoint.

As shown in Fig. 10, the movement of device in (A) is straighter than that in (B). This is because the force feedback allowed the operator to correctly recognize the movement of the device in the unintended direction. In (B), the operator was unable to recognize the origin of the StopZone and did not know how much to move the device to start the robot, which caused confusion in operation. Force feedback can be said to function effectively when moving the robot in a straight line.

2) Wall Cleaning: Fig. 11 shows the force values measured by the force sensor attached to the robot during wall cleaning, and Fig. 12 shows the torque values measured. These values can be said to be the reaction force exerted by the robot on the wall. Although the robot's performance differs depending on the control commands, there is no significant difference between the measured force and torque in (A) and (B). In (A), the operator was able to recognize that the robot was in contact with the wall through force feedback, but was confused by the vibration of the feedback, making it difficult to apply a stable force. On the other hand, in (B), the operator could recognize the contact between the robot and the wall only visually and was unable to make a confident judgment. In addition, the robot's exerted force was estimated from direct feedback such as the sound of the robot's propellers and its posture, making it difficult to apply a stable force. Therefore when the operator cannot directly monitor the work process, force feedback is considered to be able to assist in operation.

Furthermore, in the yellow region of Fig. 11 and Fig. 12, the robot is moving horizontally, and in the purple region,

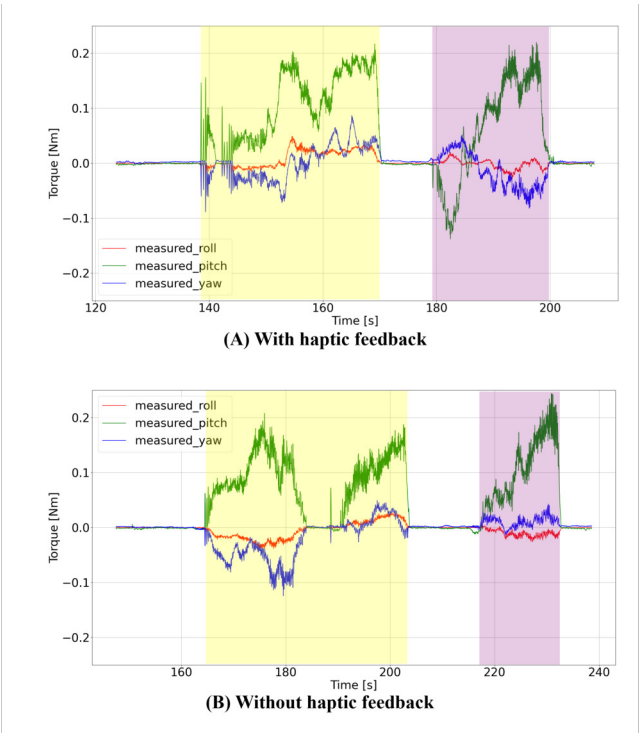

Fig. 12. Torque values measured by force sensor attached to the end effector.

it is moving vertically. In horizontal movement, yaw torque should be applied to the base of the robot's end effector, and in vertical movement, pitch torque should be applied. As shown in Fig. 12, torque in the pitch direction was measured in the purple area, but torque in the yaw direction was measured only slightly. This is thought to be because the torque in the yaw direction exceeded the limits of the robot, causing the robot to rotate. In order for the operator to correctly recognize the state of the robot and the work environment, we believe that it is necessary to generate force feedback even from such positional errors.

V. CONCLUSION

In this study, we proposed a floating teleoperation device that can independently generate all 6-dimensional forces and torques, and a teleoperation system for aerial manipulation using a fully actuated aerial robot by using this device. We also demonstrated the effectiveness of the proposed device and system through the experiment, including obstacle avoidance and tilted wall cleaning. We hope that our proposed teleoperation framework wisll improve the working capabilities of aerial robots and accelerate their use.

Future work is to evaluate the system by users and optimize the scaling parameters based on that evaluation. It is desirable to evaluate the usability of the proposed system by conducting aerial tasks remotely by multiple subjects and to reveal how to change the parameters to improve it. In addition, we aim to integrate visual feedback into the system. In this system, the operator directly monitored the work environment and the flying robot, but it is not desirable for the operator to be in the work environment in a real-world scenario. By equipping the robot with a gimbal-mounted camera and a head-mounted display for the operator, we believe that the operator will be able to correctly recognize the work environment from visual and force feedback even in situations where the operator cannot directory monitor the work environment.

REFERENCES

[1] L. Shi, N. J. H. Marcano, and R. H. Jacobsen, "A survey on multi-unmanned aerial vehicle communications for autonomous inspections," in *2019 22nd Euromicro Conference on Digital System Design (DSD)*, 2019, pp. 580–587.

[2] K. Darvish, L. Penco, J. Ramos, R. Cisneros, J. Pratt, E. Yoshida, S. Ivaldi, and D. Pucci, "Teleoperation of humanoid robots: A survey," *IEEE Transactions on Robotics*, vol. 39, no. 3, pp. 1706–1727, 2023.

[3] A. Nourmohammadi, M. Jafari, and T. O. Zander, "A survey on unmanned aerial vehicle remote control using brain-computer interface," *IEEE Transactions on Human-Machine Systems*, vol. 48, no. 4, pp. 337–348, 2018.

[4] M. Aggravi, C. Pacchierotti, and P. R. Giordano, "Connectivity-maintenance teleoperation of a uav fleet with wearable haptic feedback," *IEEE Transactions on Automation Science and Engineering*, vol. 18, no. 3, pp. 1243–1262, 2021.

[5] G. A. Yashin, D. Trinitatova, R. T. Agishev, R. Ibrahimov, and D. Tsetserukou, "Aerovr: Virtual reality-based teleoperation with tactile feedback for aerial manipulation," in *2019 19th International Conference on Advanced Robotics (ICAR)*, 2019, pp. 767–772.

[6] D. Kim and P. Y. Oh, "Testing-and-evaluation platform for haptics-based aerial manipulation with drones," in *2020 American Control Conference (ACC)*, 2020, pp. 1453–1458.

[7] M. Ryll, H. H. Bülthoff, and P. R. Giordano, "A novel overactuated quadrotor unmanned aerial vehicle: Modeling, control, and experimental validation," *IEEE Transactions on Control Systems Technology*, vol. 23, no. 2, pp. 540–556, 2015.

[8] S. Park, J. Her, J. Kim, and D. Lee, "Design, modeling and control of omni-directional aerial robot," in *2016 IEEE/RSJ International Conference on Intelligent Robots and Systems (IROS)*, 2016, pp. 1570–1575.

[9] M. Kamel, S. Verling, O. Elkhatib, C. Sprecher, P. Wulkop, Z. Taylor, R. Siegwart, and I. Gilitschenski, "The voliro omniorientational hexacopter: An agile and maneuverable tiltable-rotor aerial vehicle," *IEEE Robotics & Automation Magazine*, vol. 25, no. 4, pp. 34–44, 2018.

[10] M. Allenspach, N. Lawrance, M. Tognon, and R. Siegwart, "Towards 6dof bilateral teleoperation of an omnidirectional aerial vehicle for aerial physical interaction," in *2022 International Conference on Robotics and Automation (ICRA)*, 2022, pp. 9302–9308.

[11] M. Macchini, T. Havy, A. Weber, F. Schiano, and D. Floreano, "Hand-worn haptic interface for drone teleoperation," in *2020 IEEE International Conference on Robotics and Automation (ICRA)*, 2020, pp. 10 212–10 218.

[12] S. Heo, C. Chung, G. Lee, and D. Wigdor, "Thor's hammer: An ungrounded force feedback device utilizing propeller-induced propulsive force," in *Proceedings of the 2018 CHI Conference on Human Factors in Computing Systems*, 2018, pp. 1–11.

[13] T. Sasaki, R. S. Hartanto, K.-H. Liu, K. Tsuchiya, A. Hiyama, and M. Inami, "Leviopole: mid-air haptic interactions using multirotor," in *ACM SIGGRAPH 2018 Emerging Technologies*, ser. SIGGRAPH '18. New York, NY, USA: Association for Computing Machinery, 2018.

[14] M. Zhao, T. Anzai, F. Shi, X. Chen, K. Okada, and M. Inaba, "Design, modeling, and control of an aerial robot dragon: A dual-rotor-embedded multilink robot with the ability of multi-degree-of-freedom aerial transformation," *IEEE Robotics and Automation Letters*, vol. 3, no. 2, pp. 1176–1183, 2018.

[15] S. S. Stevens, "The psychophysics of sensory function," *Scientific American*, vol. 226, no. 6, pp. 377–386, 1957.

[16] J. Sugihara, M. Zhao, T. Nishio, K. Okada, and M. Inaba, "Beatle—self-reconfigurable aerial robot: Design, control and experimental validation," *IEEE/ASME Transactions on Mechatronics*, pp. 1–11, 2024.